Femtosecond photoelectron spectroscopy of the I_2^- anion: A semiclassical molecular dynamics simulation method

Victor S. Batista, Martin T. Zanni, B. Jefferys Greenblatt, Daniel M. Neumark, and William H. Miller
Department of Chemistry, University of California, Berkeley, California 94720
and Chemical Sciences Division, Lawrence Berkeley National Laboratory, Berkeley, California 94720

(Received 21 September 1998; accepted 9 November 1998)

In this paper we describe a new semiclassical method for simulating femtosecond pump–probe photoelectron spectroscopy, and its implementation to study the excited state photodissociation dynamics of the I_2^- anion. Our algorithm involves a forward–backward (FB) semiclassical (SC) initial value representation (IVR) method for calculating the time dependent photodetachment spectrum $P(\epsilon,\Delta t)$ as a function of the kinetic energy ϵ of the photodetached electron and the delay time Δt between the pump and probe pulses. We describe the radiation-chromophore interaction perturbatively to first order in both pulse fields, assuming the Condon approximation for the electronic transition dipole moments. Our computed spectra are in excellent agreement with full quantum mechanical simulations. © *1999 American Institute of Physics.*
[S0021-9606(99)00107-5]

I. INTRODUCTION

Ultrafast spectroscopic studies of molecular photodissociation[1–3] enable detailed experimental observation of excited state reaction dynamics occurring on a femtosecond time scale. A large number of experiments implementing ultrafast time-resolved spectroscopic techniques,[4,5] besides various types of transient absorption experiments, have been devoted to the study of ultrafast relaxation processes associated with extremely short lived excited states of polyatomic systems. Phenomena such as direct dissociation, internal conversion. vibrational energy redistribution and isomerization reactions have been explored in an effort to understand the possible mechanisms responsible for the diffuse appearance of the absorption spectra and the lack of detectable fluorescence. In particular, femtosecond photoelectron spectroscopy (FPES) has been applied to detect vibrational wave packet motion,[6–12] internal conversion[13] and photodissociation dynamics.[14–19] In contrast to most pump–probe experiments in which only absorption of the probe pulse is monitored, the FPES experiment offers the potential for following the dynamics of the entire photoexcited wave packet at each delay time without having to change the wavelength of the probe pulse. However, the interpretation of these highly multiplexed experiments can be difficult or ambiguous when the signals result from complicated dynamics involving multiple potential energy surfaces (PESs). It is essential, therefore, to develop rigorous theoretical simulation methods to provide a first principle interpretation of these state-of-the-art experiments in terms of a comprehensive understanding of the underlying dynamics. In this paper we report the development of a semiclassical method for simulating two-color pump–probe experiments of FPES. We explore the capabilities of this approach for studying the excited state photodissociation dynamics of the I_2^- anion by comparison with full-quantum mechanical calculations. This study constitutes the first application of semiclassical initial value representation (SC-IVR) methods[20–44] to the simulation of ultrafast pump–probe spectroscopy.

Experimental advances in time-resolved pump–probe spectroscopic techniques have stimulated a rapidly growing amount of theoretical and computational work, including the development of classical and semiclassical models,[45–50] one-dimensional quantum wave packet simulations,[51–54] and density-matrix formulations,[55–62] as well as theoretical studies of time resolved pump–probe ionization processes,[63–66] and the calculation of FPES signals using either approximate methods[67] where as far as the nuclear motion is concerned classical dynamics was assumed, or full-quantum mechanical formulations.[17,11,12,68–71] Exact quantum mechanical methods, however, are likely to remain of limited applicability even with projected advances in computer technologies, since they usually require significant storage space and computational effort that grows exponentially with the number of coupled degrees of freedoms. It is, thus, necessary to explore alternative computational methods which may be considered intermediate between the full-quantum mechanical and the completely classical mechanical extremes.

In recent years, there has been considerable interest in applications of SC-IVR methods to molecular dynamics (MD) simulations, including the computation of threshold photodetachment spectra[29] using a method specifically developed for the calculation of bound–bound Franck–Condon spectra.[28,40] These semiclassical techniques offered a more tractable alternative to full-quantum mechanical methods for dynamics calculations in terms of classical mechanics, but where quantum coherence and even tunneling to some extent are incorporated within the description. In a recent paper[37] we presented an implementation of a SC-IVR method[41,72] for simulating nonadiabatic photodissociation dynamics. We found that our semiclassical results were in good agreement

with full-quantum mechanical calculations, and they provided an intuitive understanding of the most fundamental dynamical features involved in the nonadiabatic process of interconversion as well as an interpretation of experimental studies of the total photoabsorption cross section as a function of the photolysis wavelength. In this article, we address the more ambitious task of computing specific two-color pump–probe experimental spectra of time-resolved FPES. We focus on the implementation of a FB/SC-IVR methodology for studying the excited state photodissociation dynamics of the I_2^- anion through FPES.

The FPES experiment involves photoexcitation of I_2^- from the ground $X\,^2\Sigma^+_{u,1/2}$ electronic state to the dissociative $A'\,^2\Pi_{1/2,g}$ PES by a 780 nm pump pulse (FWHM≈90 fs). The photoelectron spectrum of the dissociating system is measured at a series of delay times by measuring the kinetic energy of the photodetached electron when the system is photoexcited by a 260 nm probe pulse (FWHM≈100 fs) to one of the multiple electronic PESs of I_2. The variation of the photoelectron spectrum with delay time provides a description of how the local environment of the excess electron evolves in time, enabling one to monitor the dissociating anion from the initial Franck–Condon excitation region out to the asymptotic region.

Our SC-IVR method for simulating the FPES signal utilizes a standard second order perturbation treatment of the two-photon pump–probe process. The second order amplitude (first order in each of the pump and probe pulses) involves matrix elements of three successive time evolution operators; propagation forward in time on the excited A' potential energy surface (PES) of the I_2^-, propagation for a transient time on a neutral PES of I_2, and then propagation backward in time on the A' PES of I_2^-. The forward–backward (FB) aspect of the approach combines all three time evolution operators into one overall SC propagation—simply by changing the PES suddenly at each appropriate time—thus involving only a single phase space average over initial conditions (rather than a threefold phase space average if the SC-IVR were used separately for each time evolution operator). One may think of this as a more rigorous semiclassical version of the ''mixed-state propagation'' method used by Loring *et al.* in their SC-IVR calculation of photon echoes,[73] and a fully semiclassical treatment of the forward–backward idea introduced by Makri and Thompson for influence functionals.[74] The final result for the total photodetachment spectrum is obtained by summing the SC amplitude over all intermediate neutral PESs of I_2 and integrating over the transient times.

The paper is organized as follows. In Sec. II, we first outline the semiclassical approach for simulating FPES and its implementation to study the excited state photodissociation dynamics of the I_2^- anion. Section III then describes our results and compares them with the results of full-quantum mechanical calculations. Section IV summarizes and concludes.

II. METHODS

The methodology is presented in four subsections. Section II A presents the derivation of the expression for calculating the total photodetachment spectrum $P(\epsilon,\Delta t)$ as a function of the kinetic energy ϵ of the photodetached electron and the delay time Δt between pump and probe pulses. Its implementation according to a ''direct'' FB/SC-IVR method is described in Secs. II B and II E, while the corresponding SC methodology for calculating the intermediate excited state wave function is described in Sec. II C. Finally, Sec. II D describes the full quantum mechanical approach we have implemented for calculating the exact photodetachment spectrum, in order to demonstrate the accuracy and reliability of the SC results.

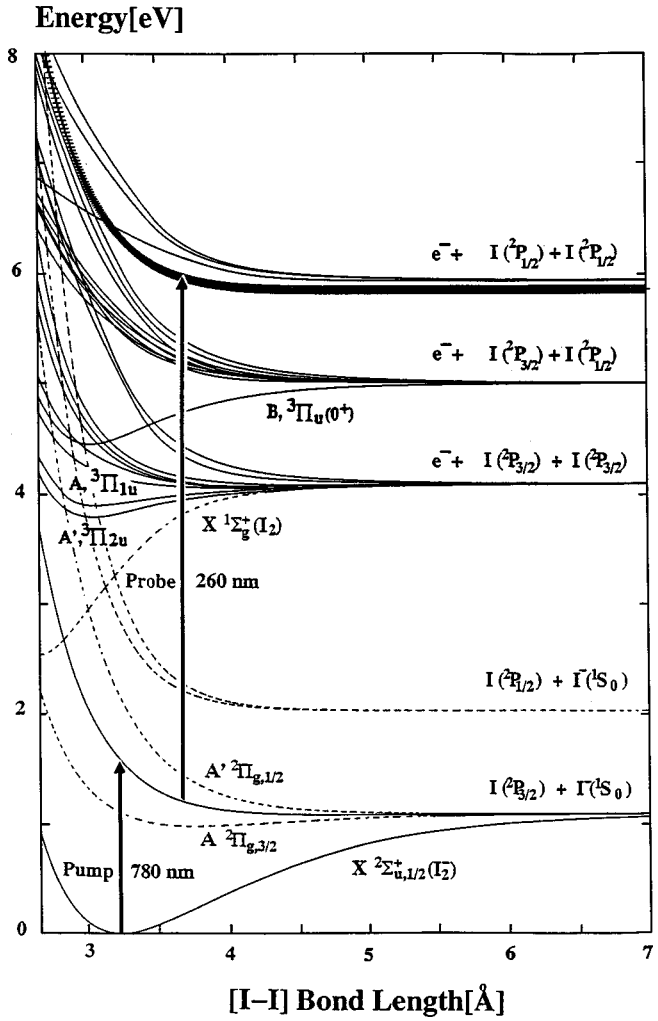

FIG. 1. Potential energy curves as a function of the I–I bond length for the 6 low-lying Hund's case (c) molecular states of I_2^- and the 23 Hund's case (c) covalent molecular states of I_2, obtained from various experiments and calculations as described in the text. Each manifold of states is labeled according to their different total angular moment dissociation products. Vertical arrows indicate experimental energies for the pump ($\lambda = 780$ nm) and probe ($\lambda = 260$ nm) pulses. The curve labeled by plus symbols corresponds to the final electronic energy as a function of the I–I bond length.

A. Time dependent photodetachment spectrum

Time-dependent photodetachment involves the two-photon pump–probe process depicted in Fig. 1; the pump pulse excites I_2^- from its ground X state to the A' excited state, and the time-delayed probe pulse photoionizes I_2^- to $I_2(K) + e^-(\epsilon)$ for various final electronic states K of I_2.

Second order time-dependent perturbation theory gives the probability of the two-photon transition as a function of time t_f,

$$P_{E_f \leftarrow E_i}(t_f) = \left| \left(-\frac{i}{\hbar} \right)^2 \int_{-\infty}^{t_f} dt \int_{-\infty}^{t} dt' e^{(i/\hbar)E_f t} \langle \Phi_f | \hat{H}_1(t) \times e^{-(i/\hbar)\hat{H}_0(t-t')} \hat{H}_1(t') | \Phi_i \rangle e^{-(i/\hbar)E_i t'} \right|^2, \tag{2.1}$$

where $\hat{H}_0$ is the (electronic and nuclear) Hamiltonian for the quantized molecular system, and $\hat{H}_1(t) = -\hat{\boldsymbol{\mu}} \cdot \boldsymbol{\epsilon}(t)$ the perturbation which couples it to the classical radiation field $\boldsymbol{\epsilon}(t)$ (within the standard dipole approximation); $|\Phi_i\rangle$ and $|\Phi_f\rangle$ are eigenstates of $\hat{H}_0$ with eigenvalues E_i and E_f, respectively.

For the present application the initial state is

$$|\Phi_i\rangle = |\phi_g\rangle |\chi_g\rangle, \tag{2.2}$$

where $|\phi_g\rangle$ is the ground (X) electronic state of I_2^- and $|\chi_g\rangle$ the ground nuclear (i.e., vibrational) state for this electronic state. Final states are of the form

$$|\Phi_f\rangle = |\phi_{K,\epsilon}\rangle |\chi_{E_K}\rangle, \tag{2.3}$$

where $|\phi_{K,\epsilon}\rangle$ is the electronic state K of I_2 with an ionized electron of kinetic energy ϵ, and $|\chi_{E_K}\rangle$ is the nuclear wave function for this state of I_2; the corresponding initial and final energies are

$$E_i = E_g,$$

$$E_f = E_K + \epsilon.$$

Since we consider only one intermediate electronic state of I_2^-, the A' excited state, the intermediate time evolution operator in the matrix element of Eq. (2.1) is

$$e^{-(i/\hbar)\hat{H}_0(t-t')} = |\phi_{A'}\rangle e^{-(i/\hbar)\hat{H}_{A'}(t-t')} \langle \phi_{A'}|, \tag{2.4}$$

where $|\phi_{A'}\rangle$ is the electronic wave function for state A' of I_2^-, and $\hat{H}_{A'}$ the nuclear Hamiltonian for this electronic state. The probability distribution of electronic kinetic energy ϵ in the long time limit, i.e., the photodetachment spectrum, is given by the sum of the above transition probability over all final electronic states K of I_2, integrated over all final nuclear states $|\chi_{E_K}\rangle$,

$$\begin{aligned} P(\epsilon) &\equiv \lim_{t_f \to \infty} \sum_K \int dE_K P_{E_K + \epsilon \leftarrow E_g}(t_f) \\ &= \sum_K \int dE_K \left| \left(-\frac{i}{\hbar} \right)^2 \int_{-\infty}^{\infty} dt \int_{-\infty}^{t} dt' (\boldsymbol{\mu}_{K,A'} \cdot \boldsymbol{\epsilon}(t)) \right. \\ &\quad \times (\boldsymbol{\mu}_{A',g} \cdot \boldsymbol{\epsilon}(t')) e^{(i/\hbar)(E_K + \epsilon)t} \\ &\quad \left. \times e^{-(i/\hbar)E_g t'} \langle \chi_{E_K} | e^{-(i/\hbar)\hat{H}_{A'}(t-t')} | \chi_g \rangle \right|^2, \end{aligned} \tag{2.5}$$

where it has been assumed that the transition dipole moments $\boldsymbol{\mu}_{K,\epsilon,A'} = \boldsymbol{\mu}_{K,A'}$ are independent of both the kinetic energy of the photodetached electron and nuclear coordinates (Condon approximation). Explicitly squaring the matrix element and using the close relation

$$\int dE_K |\chi_{E_K}\rangle \langle \chi_{E_K}| e^{-(i/\hbar)E_K(t''-t)} = e^{-(i/\hbar)\hat{H}_K(t''-t)}, \tag{2.6}$$

where $\hat{H}_K$ is the nuclear Hamiltonian for electronic state K of I_2, gives $P(\epsilon)$ as

$$\begin{aligned} P(\epsilon) = \sum_K \hbar^{-4} \int_{-\infty}^{\infty} dt \int_{-\infty}^{\infty} dt'' \int_{-\infty}^{t} dt' \int_{-\infty}^{t''} dt''' (\boldsymbol{\mu}_{K,A'} \cdot \boldsymbol{\epsilon}(t)) \\ \times (\boldsymbol{\mu}_{A',g} \cdot \boldsymbol{\epsilon}(t'))(\boldsymbol{\mu}_{K,A'} \cdot \boldsymbol{\epsilon}(t''))(\boldsymbol{\mu}_{A',g} \cdot \boldsymbol{\epsilon}(t''')) \\ \times e^{(i/\hbar)\epsilon(t-t'')} e^{-(i/\hbar)E_g(t'-t''')} \langle \chi_g | e^{-(i/\hbar)\hat{H}_{A'}(t'''-t'')} \\ \times e^{-(i/\hbar)\hat{H}_K(t''-t)} e^{-(i/\hbar)\hat{H}_{A'}(t-t')} | \chi_g \rangle. \end{aligned} \tag{2.7}$$

Equation (2.7) can also be written in terms of the trace of four successive time evolution operators

$$\begin{aligned} P(\epsilon) = \sum_K \hbar^{-4} \int_{-\infty}^{\infty} dt \int_{-\infty}^{\infty} dt'' \int_{-\infty}^{t} dt' \int_{-\infty}^{t''} dt''' (\boldsymbol{\mu}_{K,A'} \cdot \boldsymbol{\epsilon}(t)) \\ \times (\boldsymbol{\mu}_{A',g} \cdot \boldsymbol{\epsilon}(t'))(\boldsymbol{\mu}_{K,A'} \cdot \boldsymbol{\epsilon}(t''))(\boldsymbol{\mu}_{A',g} \cdot \boldsymbol{\epsilon}(t''')) \\ \times e^{(i/\hbar)\epsilon(t-t'')} \langle \chi_g | e^{-(i/\hbar)\hat{H}_X(t'-t''')} e^{-(i/\hbar)\hat{H}_{A'}(t'''-t'')} \\ \times e^{-(i/\hbar)\hat{H}_K(t''-t)} e^{-(i/\hbar)\hat{H}_{A'}(t-t')} | \chi_g \rangle. \end{aligned} \tag{2.8}$$

This would be useful if one wants to perform a *Boltzmann average* over initial vibrational states, $|\chi_g\rangle \to |\chi_{g,\nu}\rangle$, giving

$$\begin{aligned} P(\epsilon,\beta) = \sum_K \hbar^{-4} \int_{-\infty}^{\infty} dt \int_{-\infty}^{\infty} dt'' \int_{-\infty}^{t} dt' \int_{-\infty}^{t''} dt''' (\boldsymbol{\mu}_{K,A'} \\ \cdot \boldsymbol{\epsilon}(t))(\boldsymbol{\mu}_{A',g} \cdot \boldsymbol{\epsilon}(t'))(\boldsymbol{\mu}_{K,A'} \cdot \boldsymbol{\epsilon}(t''))(\boldsymbol{\mu}_{A',g} \cdot \boldsymbol{\epsilon}(t''')) \\ \times e^{(i/\hbar)\epsilon(t-t'')} Q_X^{-1} \mathrm{tr}[e^{-\beta\hat{H}_X} e^{-(i/\hbar)\hat{H}_X(t'-t''')} \\ \times e^{-(i/\hbar)\hat{H}_{A'}(t'''-t'')} e^{-(i/\hbar)\hat{H}_K(t''-t)} e^{-(i/\hbar)\hat{H}_{A'}(t-t')}], \end{aligned} \tag{2.9}$$

where $\beta = 1/k_B T$, $Q_X = \mathrm{tr}[e^{-\beta\hat{H}_X}]$, and the traces are over the nuclear degrees of freedom. Equation (2.9) thus allows one to simulate the temperature dependence of pump–probe ionization processes as an alternative to other density-matrix formulations.[58] If desirable, this can also be written as

$$P(\epsilon) = \int_{-\infty}^{\infty} dt e^{i\epsilon t} C(t), \tag{2.10}$$

where the function $C(t)$ is readily identifiable from Eqs. (2.7) and (2.9).

In the pump–probe experiment the time-dependent electric field $\boldsymbol{\epsilon}(t)$ is the sum of the two pulses,

$$\boldsymbol{\epsilon}(t) = \boldsymbol{\epsilon}_{01} F_1(t) e^{-i\omega_1 t} + \boldsymbol{\epsilon}_{02} F_2(t-\Delta t) e^{-i\omega_2(t-\Delta t)} + \text{c.c.}, \tag{2.11}$$

where $\boldsymbol{\epsilon}_{01}$ and $\boldsymbol{\epsilon}_{02}$ are constant vectors, while $F_1(t)$ and $F_2(t-\Delta t)$ describe the pump and probe pulse shapes, respectively. We have used sech^2 profiles, i.e.,

$$F_j(t) \sim \mathrm{sech}(t/(f\delta_j)), \tag{2.12}$$

where $1/f = 2\,\mathrm{sech}(\sqrt{2})$, and δ_j define the full-widths at half-maximum (FWHM), which we have chosen as $\delta_1 = 90$ fs and $\delta_2 = 100$ fs for the pump and probe pulses, respectively. Δt is the variable delay time between pump and probe pulses. Since the pump pulse is the one approximately resonant with the $A' \leftarrow X$ transition, and the probe pulse with the $(K+\epsilon) \leftarrow A'$ transition, one can to a good approximation retain only the near resonant terms in Eq. (2.7) (the rotating wave approximation), whereby $P(\epsilon)$ becomes

$$\begin{aligned} P(\epsilon,\Delta t) = \hbar^{-4} (\boldsymbol{\mu}_{A',g}\cdot\boldsymbol{\varepsilon}_{01})^2 \sum_K (\boldsymbol{\mu}_{K,A'}\cdot\boldsymbol{\varepsilon}_{02})^2 \int_{-\infty}^{\infty} dt \\ \times \int_{-\infty}^{\infty} dt'' \int_{-\infty}^{t} dt' \int_{-\infty}^{t''} dt''' e^{(i/\hbar)(\epsilon-\hbar\omega_2)(t-t'')} \\ \times e^{(i/\hbar)(E_g+\hbar\omega_1)(t'''-t')} F_1(t') F_2(t-\Delta t) F_1(t''') \\ \times F_2(t''-\Delta t) \langle \chi_g | e^{-(i/\hbar)\hat{H}_{A'}(t'''-t'')} e^{-(i/\hbar)\hat{H}_K(t''-t)} \\ \times e^{-(i/\hbar)\hat{H}'_A(t-t')} | \chi_g \rangle, \end{aligned} \tag{2.13}$$

where we have explicitly indicated the dependence of P on the delay time Δt.

Finally, we note that Eq. (2.13), or (2.7), can also be written in the equivalent form

$$P(\epsilon,\Delta t) = \lim_{t_f\to\infty} \sum_K \langle \chi_K(\epsilon,\Delta t,t_f) | \chi_K(\epsilon,\Delta t,t_f)\rangle. \tag{2.14}$$

where

$$\begin{aligned} |\chi_K(\epsilon,\Delta t,t_f)\rangle = -\frac{i}{\hbar}(\boldsymbol{\mu}_{K,A'}\cdot\boldsymbol{\varepsilon}_{02}) \int_{-\infty}^{t_f} dt' F_2(t'-\Delta t) \\ \times e^{(i/\hbar)\epsilon t'} e^{(i/\hbar)(\hat{H}_K-\hbar\omega_2)t'} |\chi_{A'}(t')\rangle, \end{aligned} \tag{2.15}$$

with

$$\begin{aligned} |\chi_{A'}(t')\rangle = -\frac{i}{\hbar}(\boldsymbol{\mu}_{A',g}\cdot\boldsymbol{\varepsilon}_{01}) \int_{-\infty}^{t'} dt F_1(t) e^{-(i/\hbar)\hat{H}_{A'}t'} \\ \times e^{(i/\hbar)(\hat{H}_{A'}-\hbar\omega_1-E_g)t} |\chi_g\rangle. \end{aligned} \tag{2.16}$$

State $|\chi_{A'}(t)\rangle$, Eq. (2.16), is the nuclear wave function for electronic state A' of I_2^- and is the result of the pump pulse which photoexcites I_2^- form its ground electronic state to the intermediate A' excited states PES, while state $|\chi_K(\epsilon,\Delta t,t_f)\rangle$, Eq. (2.15), is the result of the probe pulse excitation from the intermediate A' excited state to the final ionized state $I_2(K)+e^-(\epsilon)$. $P(\epsilon,\Delta t)$ is the norm of this latter state in the long time limit, summed over all final electronic states K. If the pump pulse were so strong as to invalidate its treatment by perturbation theory—but the perturbative treatment of the probe pulse still valid—then Eqs. (2.14) and (2.15) above would still apply, but with $|\chi_{A'}(t)\rangle$ computed nonperturbatively, e.g., by numerically solving the Schrödinger equation which couples the ground X and A' excited states of I_2^- with the time-dependent Hamiltonian $\hat{H}(t) = \hat{H}_0 - \boldsymbol{\mu}\cdot\boldsymbol{\varepsilon}_1(t)$, where $\boldsymbol{\varepsilon}_1(t)$ is the pump pulse [the first term in Eq. (2.11)]. The full quantum mechanical calculations described in Sec. II D below, and to which we compare our semiclassical calculations in Sec. III, have in fact used this approach, employing a second order differencing (SOD) scheme to solve the 2 (electronic) state Schrödinger equation with a grid to describe the nuclear (vibrational) degree of freedom. As will be seen by the comparisons in Sec. III, the perturbative treatment of the pulse is completely adequate even when the pump field depletes a significant amount of the total ground state population. In other systems, of course, this might not be true.

B. Semiclassical approach

The semiclassical calculations of the photodetachment spectrum $P(\epsilon,\Delta t)$ are based on a FB/SC-IVR implementation of Eq. (2.13), which can be written as

$$\begin{aligned} P(\epsilon,\Delta t) \sim \int_{-\infty}^{\infty} dt \int_{-\infty}^{\infty} dt'' \int_{-\infty}^{t} dt' \int_{-\infty}^{t''} dt''' F_2(t-\Delta t) \\ \times F_2(t''-\Delta t) \exp\left(\frac{i}{\hbar}\epsilon(t-t'')\right) \\ \times F_1(t') F_1(t''') \zeta_{t'''-t'',t''-t,t-t'}, \end{aligned} \tag{2.17}$$

where $F_1(t)$ and $F_2(t-\Delta t)$ are the temporal shapes of the pump and probe classical radiation pulses as defined by Eq. (2.11). The survival amplitude ζ_{t_3,t_2,t_1}, introduced by Eq. (2.17), is defined as

$$\begin{aligned} \zeta_{t_3,t_2,t_1} \equiv \sum_K (\boldsymbol{\mu}_{K,A'}\cdot\boldsymbol{\varepsilon}_{02})^2 \langle \chi_g | e^{-(i/\hbar)(\hat{H}_{A'}-\hbar\omega_1-E_g)t_3} \\ \times e^{-(i/\hbar)(\hat{H}_K-\hbar(\omega_1+\omega_2)-E_g)t_2} \\ \times e^{-(i/\hbar)(\hat{H}_{A'}-\hbar\omega_1-E_g)t_1} | \chi_g \rangle, \end{aligned} \tag{2.18}$$

and the ''forward–backward (FB)'' aspect of the present semiclassical approach is to treat the product of the three time evolution operators in Eq. (2.18) as *one* time evolution operator with the potential energy surface changing instantaneously from $V_{I_2^-}^{(A')}$ to $V_{I_2}^{(K)}$ to $V_{I_2^-}^{(A')}$ at the appropriate times (*vide infra*). Thus with the HK SC-IVR approximation[26,27] it becomes

$$\begin{aligned} \zeta_t^{\hat{HC}} = \sum_K \left(\frac{1}{2\pi\hbar}\right)^N \int_{-\infty}^{\infty} d\mathbf{p}_0 \int_{-\infty}^{\infty} d\mathbf{r}_0 C_t(\mathbf{p}_0,\mathbf{r}_0) \\ \times e^{(i/\hbar)S_t^{(K)}(\mathbf{p}_0,\mathbf{r}_0)} \Psi^{g*}(\mathbf{r}_t,\mathbf{p}_t) \Psi^g(\mathbf{r}_0,\mathbf{p}_0), \end{aligned} \tag{2.19}$$

where the index K specifies the I_2 optically active electronic state, t is the global time determined by the time intervals t_1, t_2 and t_3 introduced by Eq. (2.18), while $\Psi^g(\mathbf{r},\mathbf{p})$ is the coherent state transform of the initial nuclear wave function $\langle \mathbf{r}|\chi_g\rangle$,

$$\Psi^g(\mathbf{r},\mathbf{p}) = \langle g_{\mathbf{p},\mathbf{r}} | \chi_g \rangle. \tag{2.20}$$

In the present case $N=1$ and defines the number of nuclear coordinates. The formulation is presented, however, in multidimensional notation for systems with an arbitrary number

of nuclear coordinates. The nuclear wave function that represents the initial population in the X PES of I_2^- is assumed to be its ground vibrational state,

$$\langle \mathbf{r}|\chi_g\rangle = \left(\frac{\alpha}{\pi}\right)^{1/4} \exp\left(-\frac{\alpha}{2}(\mathbf{r}-\mathbf{r}_{\rm eq})^2\right), \tag{2.21}$$

where $\mathbf{r}$ is the I–I bond length, and $\mathbf{r}_{\rm eq}$ its equilibrium value, $\alpha=\sqrt{\kappa\mu/\hbar^2}$, where κ is the vibrational harmonic constant of the molecule in its ground electronic state, and μ is the reduced mass. This initial wave function is constructed on the basis of the low temperature approximation, i.e., assuming that contributions from anharmonicity and higher vibrational levels can be neglected. The functions $\langle \mathbf{r}|g_{\mathbf{r}_t,\mathbf{p}_t}\rangle$ are Gaussian wave packets (minimum uncertainty wave packets, or coherent states),

$$\begin{aligned}\langle \mathbf{r}|g_{\mathbf{r}_t,\mathbf{p}_t}\rangle &= g_{\mathbf{r}_t,\mathbf{p}_t}(\mathbf{r}) \\ &= \prod_{j=1}^{N}\left(\frac{2\gamma(j)}{\pi}\right)^{1/4} \\ &\quad \times e^{-\gamma(j)[r(j)-r_t(j)]^2+(i/\hbar)p_t(j)[r(j)-r_t(j)]},\end{aligned} \tag{2.22}$$

where $\gamma(j)$ are constant parameters. The integration variables $(\mathbf{p}_0,\mathbf{r}_0)$ in Eq. (2.19) are the initial conditions for classical trajectories of the time-evolved coordinates and momenta, $\mathbf{r}_t\equiv\mathbf{r}_t(\mathbf{p}_0,\mathbf{r}_0)$ and $\mathbf{p}_t\equiv\mathbf{p}_t(\mathbf{p}_0,\mathbf{r}_0)$, obtained by integrating the usual classical equations of motion. $S_t^{(K)}(\mathbf{p}_0,\mathbf{r}_0)$ is the classical action along this trajectory, obtained by integrating the following equation:

$$\frac{dS_t^{(K)}}{dt} = \mathbf{p}_t\cdot\dot{\mathbf{r}}_t - H^{(K)}(\mathbf{p}_t,\mathbf{r}_t,t), \tag{2.23}$$

for the global time range defined by the forward t_1, transient t_2 and backward t_3 time increments. The Hamiltonian $H^{(K)}(\mathbf{p}_t,\mathbf{r}_t,t)$ in Eq. (2.23) above, is the time dependent Hamiltonian for nuclear coordinates and momenta,

$$H^{(K)}(\mathbf{r}_t,\mathbf{p}_t,t) = \frac{\mathbf{p}_t^2}{2m} + V^{(K)}(\mathbf{r}_t,t), \tag{2.24}$$

where the time dependent potential $V^{(K)}(\mathbf{r}_t,t)$ for the FB trajectory is given explicitly by

$$V^{(K)}(\mathbf{r}_t,t) = \begin{cases} V_{I_2^-}^{(A')}(\mathbf{r}_t)-\hbar\omega_1-E_g, & 0<t<t_1 \\ V_{I_2}^{(K)}(\mathbf{r}_t)-\hbar(\omega_1+\omega_2)-E_g, & t_1<t<t_1+t_2 \\ V_{I_2^-}^{(A')}(\mathbf{r}_t)-\hbar\omega_1-E_g, & t_1+t_2<t<t_1+t_2+t_3, \end{cases} \tag{2.25}$$

where $V_{I_2^-}^{(A')}$ and $V_{I_2}^{(K)}$ are the indicated Born–Oppenheimer PESs of I_2^- and I_2, respectively. The pre-exponential factor in the integrand of Eq. (2.19) is given by

$$C_t(\mathbf{p}_0,\mathbf{r}_0) = \sqrt{\det[\mathbf{M}]}, \tag{2.26}$$

where $\mathbf{M}$ is a linear combination of components of the monodromy matrix,

$$\begin{aligned}M(j,k) = \frac{1}{2}\Bigg(&\frac{\partial r_t(k)}{\partial r_0(j)} + \frac{\gamma(j)}{\gamma(k)}\frac{\partial p_t(k)}{\partial p_0(j)} - \frac{1}{2i\hbar\gamma(k)}\frac{\partial p_t(k)}{\partial r_0(j)} \\ &- 2i\hbar\gamma(j)\frac{\partial r_t(k)}{\partial p_0(j)}\Bigg),\end{aligned} \tag{2.27}$$

where $\gamma(j)$ are the constant parameters in the Gaussian wave packets of Eq. (2.22). The various time dependent partial derivatives are obtained by numerical integration of the following equations for the stability matrix,

$$\begin{aligned}\frac{d}{dt}\left(\frac{\partial p_t(i)}{\partial z(j)}\right) &= -\sum_{l=1}^{N}\Bigg(\frac{\partial^2 H^{(K)}(\mathbf{p}_t,\mathbf{r}_t,t)}{\partial p_t(l)\partial r_t(i)}\frac{\partial p_t(l)}{\partial z(j)} \\ &\quad + \frac{\partial^2 H^{(K)}(\mathbf{p}_t,\mathbf{r}_t,t)}{\partial r_t(l)\partial r_t(i)}\frac{\partial r_t(l)}{\partial z(j)}\Bigg), \\ \frac{d}{dt}\left(\frac{\partial r_t(i)}{\partial z(j)}\right) &= +\sum_{l=1}^{N}\Bigg(\frac{\partial^2 H^{(K)}(\mathbf{p}_t,\mathbf{r}_t,t)}{\partial p_t(l)\partial p_t(i)}\frac{\partial p_t(l)}{\partial z(j)} \\ &\quad + \frac{\partial^2 H^{(K)}(\mathbf{p}_t,\mathbf{r}_t,t)}{\partial r_t(l)\partial p_t(i)}\frac{\partial r_t(l)}{\partial z(j)}\Bigg),\end{aligned}$$

where $z=p_0$ or r_0.

Trajectories are initialized in our simulations through MC sampling of coordinates and momenta according to localized phase space distributions determined by the coherent state transforms of excited state populations defined by Eq. (2.20). The partial contribution of a single trajectory to the photodetachment spectrum $P(\epsilon,\Delta t)$ requires forward propagation on the A' excited state PES of I_2^- form the initial phase point $(\mathbf{p}_0,\mathbf{r}_0)$ to the resulting phase point $(\mathbf{r}_{t_1},\mathbf{p}_{t_1})$ at time $t_1=t-t'$, then—with the trajectory being continuous at the transition—propagation for a time $t_2=t''-t$ on the K excited state PES of I_2, and finally propagation for a time $t_3=t'''-t''$ once again on the A' PES of I_2^-. The time intervals that make the most important contribution to the overall integral are selected through MC sampling of times t, t', t'', and t''', according to the distributions determined by the intensity profiles F_1 and F_2 characterizing the pump and probe laser fields. This importance sampling technique is ideally suited for calculating high-dimensional integrals.

The computational task is thus reduced to the evaluation of a multidimensional integral whose dimension grows only linearly with the number of coupled degrees of freedom. This integral results from substituting Eq. (2.19) into Eq. (2.17), and is evaluated for the whole range of electronic kinetic energies values ($0\,\text{eV}\leqslant\epsilon\leqslant 3\,\text{eV}$), at each delay time Δt. Since this calculation involves a single phase space integral over initial conditions, and the action integral is obtained from integrating Eq. (2.23) according to a forward and backward time increment associated with dynamics in the A' electronic excited state of I_2^- [with a transient propagation in the neutral $V_{I_2}^{(K)}$ state PES], the oscillatory character of the integrand is expected to be much less than for a triple phase space integral defined by three separate time evolution operators. For the same reason, the pre-exponential factor is

also expected to be better behaved, defining a SC integration scheme that is probably as simple and efficient as one can expect. The final FPES signals are calculated from the convolution of $P(\epsilon,\Delta t)$ with the instrument resolution function, obtained from the experimental I^- photoelectron spectrum.

Trajectories are independent of each other and, therefore, computed in parallel. This computation is performed with the same programming model as described in our previous work,[37] according to a portable single program multiple data streams (SPMD) code that runs under the message passing interface (MPI) environment and is optimized for nodes that are relatively powerful. At the hardware level we thus have coarse-grained parallelism, allowing us to allocate hundreds or thousands of trajectories per node, minimizing communication costs on the parallel architecture. This trivial parallelization strategy exploits the benefit of having initial states described by localized phase space distributions as well as perturbation pulse fields of ultrafast femtosecond spectroscopy that are localized in time.

C. Semiclassical excited state wave function

The FB/SC-IVR method for computing the time dependent photodetachment spectrum, described in Sec. II B, is a direct approach based on standard time-dependent perturbation theory (first order in both pulse fields) which does not require the computation of the A' excited state wave function $|\psi_{A'}\rangle$. This quantity, however, can also be obtained at the same level of theory through the implementation of Eq. (2.16) according to the SC-IVR methodology described in this section. This equation can be written as

$$\langle \mathbf{r}|\chi_{A'}(t'')\rangle = -\frac{i}{\hbar}(\boldsymbol{\mu}_{A',g}\cdot\boldsymbol{\varepsilon}_{01})\int_{-\infty}^{t''} dt' F_1(t')\Theta_{t',t''}(\mathbf{r}), \tag{2.28}$$

where $\mathbf{r}$ are the nuclear coordinates and $F_1(t')$ is the sech^2 temporal profile of the pump pulse, introduced by Eq. (2.11). $\Theta_{t',t''}(\mathbf{r})$ is defined as

$$\Theta_{t',t''}(\mathbf{r}) = \langle \mathbf{r}|e^{-(i/\hbar)\hat{H}_{A'}t''}e^{(i/\hbar)(\hat{H}_{A'}-\hbar\omega_1-E_g)t'}|\chi_g\rangle, \tag{2.29}$$

and with the HK SC-IVR approximation[26,27] becomes

$$\Theta_t^{HC}(\mathbf{r}) = \left(\frac{1}{2\pi\hbar}\right)^N \int_{-\infty}^{\infty} d\mathbf{p}_0 \int_{-\infty}^{\infty} d\mathbf{r}_0 C_t(\mathbf{p}_0,\mathbf{r}_0) \times e^{(i/\hbar)S_t(\mathbf{p}_0,\mathbf{r}_0)} g_{\mathbf{r}_t,\mathbf{p}_t}(\mathbf{r})\Psi^g(\mathbf{r}_0\cdot\mathbf{p}_0), \tag{2.30}$$

where t is the global time determined by the time intervals t' and t'', introduced by Eq. (2.29), and N defines the number of nuclear coordinates. $\Psi^g(\mathbf{r},\mathbf{p})$ is the coherent state transform of the initial nuclear wave function $\langle \mathbf{r}|\chi_g\rangle$, defined according to Eq. (2.20), while $g_{\mathbf{r}_t,\mathbf{p}_t}(\mathbf{r})$ are the minimum uncertainty wave packets defined by Eq. (2.22).

Following the methodology presented in Sec. II B, the excited state wave function $\langle \mathbf{r}|\chi_{A'}(t'')\rangle$ is computed at time t'' by combining the two time evolution operators of Eq. (2.29) into a single phase space integral described by Eqs. (2.30) and (2.28). Initial phase points $(\mathbf{p}_0,\mathbf{r}_0)$ and propagation times t' are selected through MC sampling, according to the distributions $\Psi^g(\mathbf{r},\mathbf{p})$ and $F_1(t')$, respectively. Individual trajectories propagate from their initial phase points $(\mathbf{p}_0,\mathbf{r}_0)$ to the resulting phase points $(\mathbf{r}_{t'},\mathbf{p}_{t'})$, at time t', according to the shifted PES $V(\mathbf{r}_t,t)=V_{I_2^-}(\mathbf{r}_t)-\hbar\omega_1-E_g$. This initial propagation period is then followed by the evolution of the system for a time t'', according to the unshifted PES $V(\mathbf{r}_t,t)=V_{I_2^-}(\mathbf{r}_t)$, with $(\mathbf{r}_{t'},\mathbf{p}_{t'})$ being continuous at the transition.

This semiclassical wave function $|\psi_{A'}\rangle$ certainly incorporates the dynamical effects of the finite pulse duration since the 90 fs pump pulse is long in comparison to the excited state photodissociation dynamics, which proceeds within this time scale while population is still being fed into the excited state PES. However, it does not incorporate the possible dynamical effects which result from the perturbation of the ground state wave function by the pump pulse. In principle, these effects can be important when the intensity of the perturbational field is so large that a significant fraction of the population is transferred to the excited state. The comparison presented in Sec. III, between the semiclassical wave function $|\psi_{A'}\rangle$ and the exact full-quantum mechanical results, provides a useful test of both the perturbation theory approximations made for the calculation of the complete photodetachment spectra and the ability of our SC approach for modeling excited state photodissociation dynamics.

D. Full-quantum mechanical implementation

Full-quantum mechanical calculations of the photodetachment spectra $P(\epsilon,\Delta t)$ are based on Eq. (2.14). This equation can be written as a double space integral

$$\begin{aligned} P(\epsilon,\Delta t) = {} & \hbar^{-4}(\boldsymbol{\mu}_{A',g}\cdot\boldsymbol{\varepsilon}_{01})^2 \\ & \times\sum_K (\boldsymbol{\mu}_{K,A'}\cdot\boldsymbol{\varepsilon}_{02})^2 \int_{-\infty}^{\infty} dt' \int_{-\infty}^{\infty} dt'' e^{i\epsilon(t'-t'')/\hbar} \\ & \times F_2(t''-\Delta t)F_2(t'-\Delta t) \\ & \times\langle \chi_{A'}(t'')|e^{i(\hat{H}_K-\hbar\omega_2)(t'-t'')/\hbar}|\chi_{A'}(t')\rangle, \end{aligned} \tag{2.31}$$

and evaluated as the one-dimensional Fourier transform

$$\begin{aligned} P(\epsilon,\Delta t) = {} & \hbar^{-4}(\boldsymbol{\mu}_{A',g}\cdot\boldsymbol{\varepsilon}_{01})^2 \sum_K (\boldsymbol{\mu}_{K,A'}\cdot\boldsymbol{\varepsilon}_{02})^2 \\ & \times\int_{-\infty}^{\infty} dT e^{i\epsilon T/\hbar}\left[\int_{t_{\min}}^{t_{\max}} dt'' F_2(t''-\Delta t) \right. \\ & \left. \times F_2(T+t''-\Delta t)\langle \chi_K(t'',T)|\chi_{A'}(t'+T)\rangle\right], \end{aligned} \tag{2.32}$$

where $T=t'-t''$ and $|\chi_K(t'',T)\rangle = e^{-i(\hat{H}_K-\hbar\omega_2)T/\hbar}|\chi_{A'}(t'')\rangle$, while $t_{\min}$ and $t_{\max}$ replace the infinite integral limits of t'' in Eq. (2.31) since, in general, dynamics needs to be propagated only for a finite time range. $|\chi_{A'}\rangle$ is obtained according to a grid based second-order differencing scheme (SOD),[75] by numerically integrating the Schrödinger equation with a time dependent perturbation field $\boldsymbol{\epsilon}(t)$ defined according to the rotating wave approximation (RWA), $\boldsymbol{\epsilon}(t)=\boldsymbol{\epsilon}_{01}F_1(t)e^{-i\omega_1 t}$,

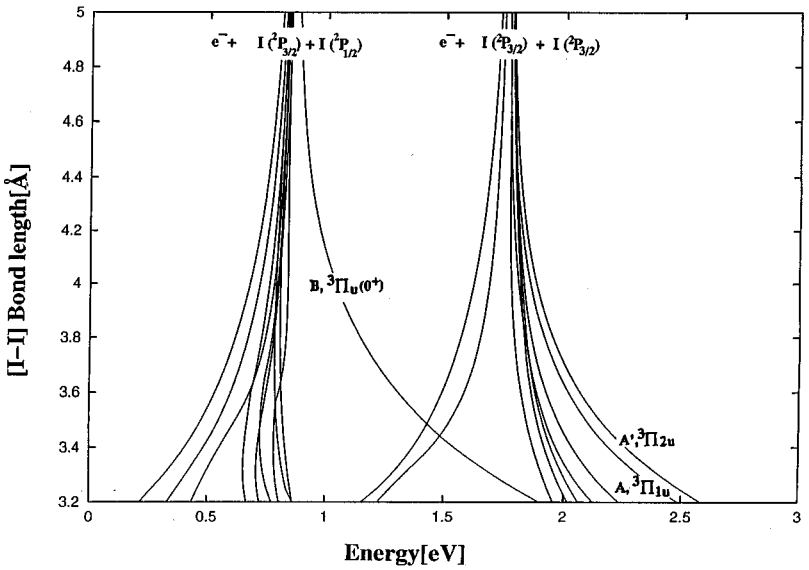

FIG. 2. Kinetic energy of the photodetached electron for each of the possible I_2 final states, as a function of the I–I bond length in an inverted plot.

and a value for dipole moment of transition $\mu_{g,A'}$ adjusted to approximately match the experimentally observed depletion of ground electronic state population. Most of the computational effort involves propagation the nuclear wave function $|\chi_K\rangle$ on the neutral I_2 excited state PES labeled by index K, which is computed concurrently with $|\chi_{A'}\rangle$. The overlap integrals $O(t'',T)=\langle\chi_K(t'',T)|\chi_{A'}(t''+T)\rangle$ are stored over the course of the anion excited state propagation as a function of t'', for only the $0-n\delta_2$ range of T (with $n\approx 3$), minimizing the computational effort and storage space requirements as an improved version of previous full-quantum mechanical simulations.[17] These matrix elements $O(t'',T)$ are subsequently used for evaluating the integral over t'' in Eq. (2.32) and the Fourier transform over T for calculating the entire photoelectron spectrum at arbitrary delay time Δt. Perhaps the most important advantage of this particular full-quantum mechanical implementation method is the significant optimization in storage space requirements relative to other techniques that might require storage space for the excited state wave function, scaling with the size of the grid and the dimensionality of the configurational space. The same computational approach also allows for simulating full quantum-dynamics in the weak-field limit, by propagating the excited state wave function component with the constraint of stationary state character for the ground wave function component.

E. Potential energy surfaces

The ground electronic state of I_2^- is described according to Ref. 8, while the excited state PESs of I_2^- are described according to the empirical PESs of Ref. 76. These approximate excited state PESs are constructed from an assortment of experimental data including Raman spectroscopy in matrices, electronic spectroscopy in crystals and gas-phase dissociative attachment experiments. A discussion of other possible choices, including empirical[77,78] or theoretical[79–82] I_2^- PESs is presented in Ref. 8, where accurate corrections to the X ground state PES are reported from experiments that involve a combination of conventional and femtosecond photoelectron spectroscopic techniques.

Figure 1 shows the PESs involved in our simulations (solid curves) including the ground state X and excited state A' PESs within the manifold of 6 low-lying Hund's case (c) molecular states of I_2^-, as well as the 23 Hund's case (c) covalent molecular states of I_2 obtained from experimental studies,[83–90] or approximate theoretical calculations,[91–94] as functions of the I–I bond length. The manifolds of states are labeled by their atomic dissociation states, and the final energy $E^{(e)}=V_{I_2}^{(K)}+\epsilon$ is represented by the curve labeled by plus symbols. Figure 2 shows, as a rotated plot, the possible values of electronic kinetic energy $\epsilon=V_{I_2^-}^{(A')}(\mathbf{r}_t)+\hbar\omega_2-V_{I_2}^{(K)}(\mathbf{r}_t)$ as a function of the I–I bond length $\mathbf{r}_t$, assuming

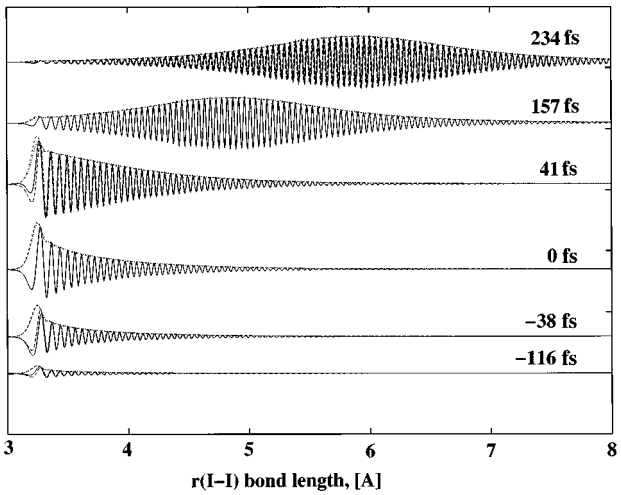

FIG. 3. Comparison of the real part (solid lines) and modulus (short dashes) of the semiclassical excited state wave function $\langle\mathbf{r}|\chi_{A'}\rangle$, with the corresponding real part (long dashes) and modulus (dots) obtained according to full-quantum mechanical calculations.

a classical description for the nuclear motion, and the Franck–Condon approximation.

There is, however, a considerable degree of uncertainty in the PESs of this system. The I_2^- PESs are still the subject of current investigations and some of the I_2 excited state PESs are not well known experimentally, including most of the states that dissociate to $I(^2P_{3/2})+I(^2P_{1/2})$, and are described here by curves obtained from theoretical calculations. Unfortunately, the dipole operator matrix elements between the I_2 and I_2^- excited state PESs are also not available. Having these limitations in the description of the electronic structure, there is no adequate way of simulating the complete photodetachment spectrum without relying on approximate PESs and a model for the transition dipole moments. In order to make a rigorous comparison of our semiclassical results with full-quantum mechanical calculations we analyze first the contribution of a single state of I_2 to the photodetachment spectra, calculated according to the Condon approximation. After demonstrating the accuracy and reliability of our SC calculations for a single state, we present the SC results for the photodetachment spectra summed over all final states of I_2 obtained according to a simple model for the transition dipole moments, which are assumed to be constant and independent of nuclear coordinates and electronic kinetic energy of the photodetached electron.

III. RESULTS

We present our results in three subsections. Section III A presents the comparison between the SC excited state wave functions, obtained according to the methodology presented in Sec. II C, and the corresponding full-quantum mechanical calculations obtained according to the method described in Sec. II D. Section III B then compares the SC photodetachment spectrum obtained according to the FB/SC-IVR methodology presented in Sec. II B with the corresponding results obtained according to the full-quantum mechanical approach presented in Sec. II D, both for a single state of I_2. Finally, Sec. III C presents SC results for the complete photodetachment spectra (i.e., summed over all final states of I_2) obtained according to a simple model for the transition dipole moments. All SC results were converged with less than 10^6 trajectories, which were integrated according to a standard fourth-order Runge–Kutta algorithm,[95] with a 0.125 fs integration step, using the parallel programming model described in Sec. II B. The values of $\gamma(j)$, introduced by Eq. (2.22), were set equal to the values of $\alpha(j)$, introduced by Eq. (2.21).[37] All forces and second derivatives necessary for integrating the equations of motion were calculated using finite difference expressions.

A. Comparison between SC and full-quantum mechanical excited state wave functions

Figure 3 shows the real part and modulus of the semiclassical excited state wave function $\langle \mathbf{r}|\chi_{A'}\rangle$ obtained according to the methodology presented in Sec. II C, and the corresponding full-quantum mechanical results obtained at the first-order perturbation level of theory, as described in Sec. II D. This figure shows that the SC propagation of the excited state wave function is in excellent agreement with

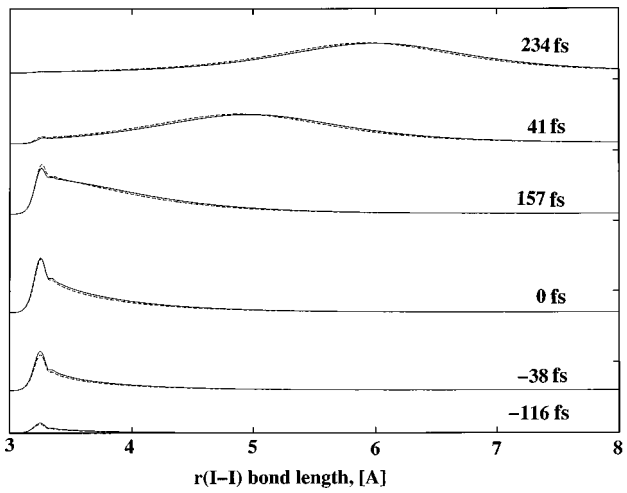

FIG. 4. Comparison of the full-quantum mechanical wave functions, obtained at the first-order perturbation level of theory (long dashes) and allowing for 40% depletion of the ground state population as described in the text (solid lines).

the corresponding full-quantum mechanical evolution for all times, as determined by the dissociative character of the A' excited state PES and the sech^2 profile of the (FWHM=90 fs) pump pulse. At the shortest time presented in this figure ($t=-116$ fs) the excited state wave function is localized at the FC region with a maximum amplitude at the geometry that satisfies the resonance condition. At longer times ($t=-38-0$ fs), it becomes progressively more peaked at the geometry that satisfies the resonance condition while its tail becomes more prominent and extends out to longer internuclear distances as the excited state population moves from the FC region out to the asymptotic region. At early positive times ($t=41$ fs), the peak at the resonance condition ($r\approx 3.205$ Å) decreases with the pump pulse intensity, while the tail involves most of the excited state population and continues spreading out. At longer times ($t=157-234$ fs), the peak at the FC region becomes much smaller, while the excited state wave packet moves towards larger internuclear geometries. This almost perfect agreement between the SC and full-quantum mechanical results demonstrates the capabilities of the SC approach to provide a tractable alternative to full quantum mechanical techniques, specifically designed to simulate finite pulse duration effects on the evolution of an excited state wave function undergoing ultrafast relaxation dynamics within the time scale of the pulsewidth. However, there is the nontrivial question as to how important are the dynamical effects neglected by a formulation based on first order perturbation theory that might affect the propagation of the excited state wave function when the (FWHM=90 fs) pump pulse is so intense that depletes a significant amount of the ground state population.

Figure 4 shows the comparison of the SC results presented in Fig. 3 with the exact full-quantum mechanical calculations obtained by integrating the time dependent Schrödinger equation allowing for an integrated depletion of the ground electronic state population of about 40%, as suggested by typical experimental reductions of the integrated ground electronic state photodetachment intensities in the

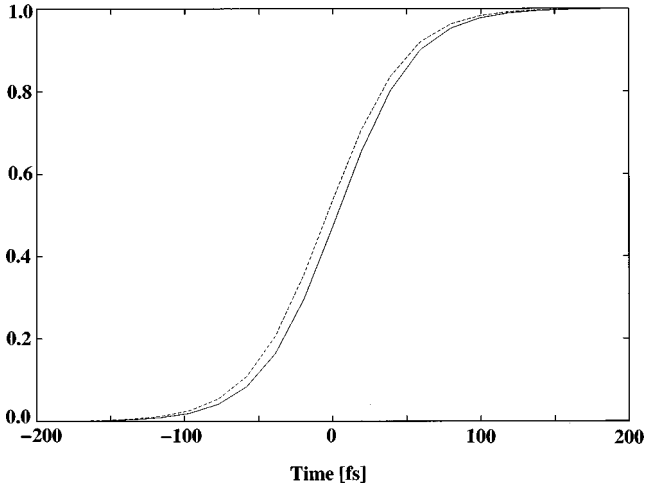

FIG. 5. SC (solid line) and full-quantum mechanical (long dashes) integrated excited state populations as a function of time relative to the center of the pump pulse.

presence of the pump pulse. This figure shows that there is only a very small perturbational effect on the dynamics of the excited state wave function, which involves an approximately 7 fs time shift, while the overall shape amplitude and phase remain unchanged. It is, thus, reasonable to expect that the SC-IVR formulation based on first-order perturbation theory should be able to describe accurately the complete photodetachment spectra as modulated by the pump and probe pulse profiles, even when the pump field is so intense that depletes 40% of the total ground state population. For the sake of completeness, we present in Fig. 5 the SC and exact full-quantum mechanical integrated excited state populations, for the whole range of times. This figure shows that except for the approximately 7 fs time shift, there is almost perfect agreement between the SC and full-quantum mechanical excited state population risetime throughout the complete photolysis event.

B. Comparison between SC and full-quantum mechanical photodetachment spectra

In order to make a rigorous comparison between SC and full-quantum mechanical photodetachment spectra, Fig. 6 compares an individual I_2 electronic excited state contribution to the photodetachment spectrum, obtained according to Eq. (2.17) where the sum over electronic states K is limited to a single term (the A electronic state of I_2). Figure 7 shows the convoluted signals, according to a typical instrument resolution function. We focus on the contributions of scattering events to the A excited state PES of I_2 calculated within the Condon approximation, as described in Secs. II B and II D, for the $-100-100$ fs range of delay times where changes of intensities are more significant. In contrast to the analysis of the complete photodetachment spectra, this comparison of a single state component allows one to check the accuracy and reliability of the FB/SC-IVR method to reproduce the exact quantum mechanical contributions of an individual I_2 state to the distribution of intensities in the photodetachment spectra, as a function of ϵ and Δt.

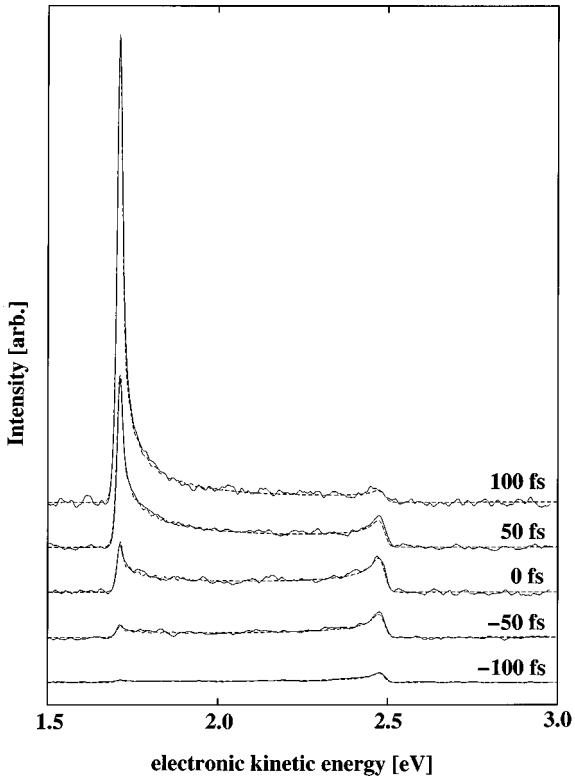

FIG. 6. Comparison between SC (solid lines) and full-quantum mechanical (long dashes) individual A state component contribution to the photodetachment spectrum, as a function of kinetic energy ϵ of the photodetached electron for delay times $\Delta t = -100, -50, 0, 50, 100$ fs between pump and probe pulses.

The first feature to note when comparing our calculated signals with full-quantum mechanical results is that the overall shapes of the spectra, and the trend in these shapes with delay time Δt is well reproduced by our SC calculations. At the longest delay time ($\Delta t = 100$ fs), for example, the signals consist of a sharp peak at $\epsilon \approx 1.7$ eV, characteristic of the I^- spectrum. This signal corresponds approximately to the photodetachment spectrum at longer times, when dissociation to $I^- + I$ is complete and photodetachment takes place from the free I^- ion. At the shortest delay time ($\Delta t = -100$ fs), the semiclassical and quantum mechanical signals again agree with one another quite accurately and show qualitatively different behavior from that observed at longer Δt. The first major difference to note is that the sharp peak at $\epsilon \approx 1.7$ eV, characteristic of separated photofragments, is now almost completely absent and the spectrum is peaked at $\epsilon \approx 2.5$ eV instead, since photodetachment takes place primarily from the FC region with this predominant kinetic energy component. At intermediate delay times the features outlined above for the $\epsilon \approx 1.7$ eV band merge continuously from one extreme to the other, monotonically increasing the I^- signal with Δt, as the I_2^- undergoes complete dissociation. On the other hand, the peak at $\epsilon \approx 2.5$ eV reaches its maximum at $\Delta t = 0.0$ fs and gradually dies out at longer delay times. Hence the distribution of intensities of an individual I_2 state component contribution to the total photoelectron spectrum changes significantly with delay time, and the description of these changes given by the FB/SC-IVR method, presented in

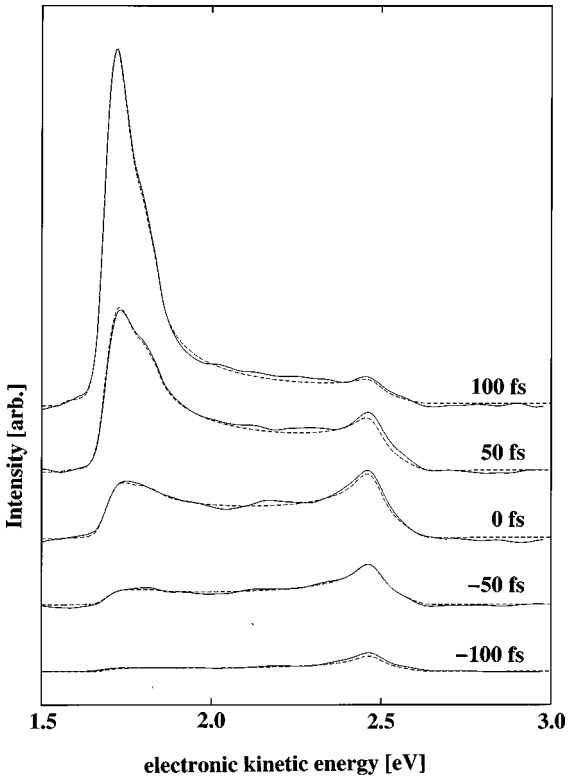

FIG. 7. Same as Fig. 6, but convoluted according to a typical instrument resolution function.

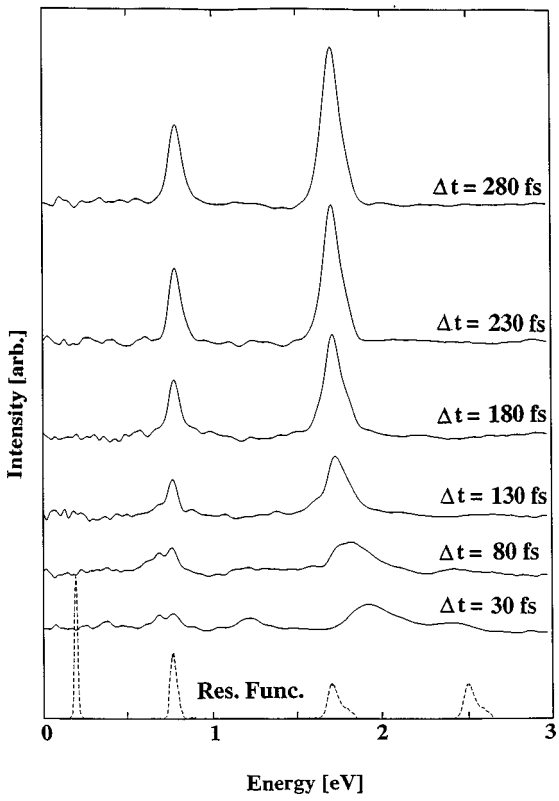

FIG. 8. Complete SC photodetachment spectra, convoluted according to a typical instrument resolution function presented at the bottom of the figure at four different energies (the convolution function at other energies is obtained by interpolation).

Sec. II B, is in excellent agreement with full-quantum mechanical calculations.

C. Complete photodetachment spectra

Figure 8 presents the complete SC photodetachment spectra which results from all possible excitations into the optically allowed and energetically accessible I_2 excited state PESs, convoluted according to a typical instrument resolution function. The comparison between the complete photodetachment spectra and the corresponding experimental signals suggests corrections for possible inaccuracies of the empirical excited state PESs employed in our simulations. However, the presentation in this section concerns only with a discussion of the SC results, leaving the scomparison with experimental data as the subject of the following article. In analogy to the individual contribution to the photodetachment spectrum of the *A* state of I_2 presented in Sec. III B, the complete photodetachment spectrum at long delay times converges asymptotically to the I^- photodetachment spectrum. However, in addition to the $\epsilon \approx 1.7$ eV band, characteristic of the (3/2,3/2) I_2 ground state dissociation limit, the complete photodetachment spectrum includes the other atomic band at $\epsilon \approx 0.8$ eV, characteristic of photofragmentation into the excited (3/2,1/2) manifold of atomic states (see Fig. 2). For shorter delay times, these two sharp atomic bands transform into broad and structureless signals characteristic of photodetachment to molecular excited state PESs of diverse symmetry and topology. This spectroscopic broadening is more significant for the high energy band which at short delay times extends from ~1.2 eV to ~2.5 eV, as determined by the dispersion of electronic states in the low lying manifold of PESs (see Fig. 2). Furthermore, the low energy band also transforms at shorter times from a sharp atomic signal to a much wider band in the ~0.5–1.0 eV range of electronic kinetic energies, as the *B* electronic state separates from the excited state manifold of PESs which disperses within this 0.5 eV range of kinetic energy values at shorter internuclear distances (see Fig. 2).

As presented in Sec. II E, these SC simulations of the complete photodetachment spectra were performed assuming that transitions from the $A'\,^2\Pi_{1/2,g}$ excited electronic state of I_2^- to all of the I_2 electronic excited states were allowed with transition dipole moments that were constant as functions of the I–I bond length (Condon approximation), and adjusted to match approximately the relative intensities of the $^2P_{1/2}$ and $^2P_{3/2}$ experimental bands. The transition dipole moment to the I_2 ground state, $X\,^1\Sigma_g^+ \leftarrow A'\,^2\Pi_{1/2,g}$ was assumed to vanish because of symmetry. In principle, one could have an estimate of the relative importance of the different transitions from the analysis of the corresponding electronic configurations, defined according to the simplest LCAO approximation for the valence-shell molecular orbitals in the uncoupled representation.[94] However, a rigorous model for the actual transition dipole moments would necessarily require ab-initio or empirical information, since spin–orbit coupling in I_2 and I_2^- is so important that the *l* and *m* quantum numbers which define the approximate electronic configurations in the uncoupled representation are actually ill-defined, and the

only well defined quantum number in these systems is the projection of the total angular momentum Ω in the direction of the bond.

IV. CONCLUSIONS

We have shown in this paper how the FB/SC-IVR method can be used to simulate femtosecond pump–probe photoelectron spectroscopy. This approach reduces the calculation of the photodetachment spectrum to the evaluation of a single phase space average over the initial conditions of classical trajectories, a computation that scales linearly with the number of coupled degrees of freedom and for which MC importance sampling techniques are readily available.

We have demonstrated the capabilities of the FB/SC-IVR method for simulating the ultrafast photodissociation dynamics of a realistic reaction, showing excellent agreement with full-quantum mechanical calculations in describing all features in the photoelectron spectrum. It was also seen to produce results for the wave function on the photoexcited intermediate (A') state of I_2^- in good agreement with non-perturbative full-quantum mechanical calculations.

The accuracy and reliability of the FB/SC-IVR approach give us confidence that it will also provide a good description of the analogous ultrafast relaxation processes involved in two-color pump–probe experiments of FPES in more complex molecular systems, for which a full quantum treatment would be out of the question. In future applications, we will implement the present FB/SC-IVR method on higher dimensionality problems. Of particular interest would be to extend the present semiclassical methodology to incorporate the dynamical effects of electronic nonadiabaticity in the same I_2^- system but clustered with solvent molecules or in a condensed phase environment. These effects have already been observed in nonadiabatic MD simulations of the photodissociation and geminate recombination dynamics of I_2 (Refs. 96 and 97) and I_2^-,[98,67] where the presence of a surrounding molecular environment significantly perturbed the excited state PESs that participated in the relaxation dynamics and induced nonadiabatic transitions between them. According to the present application, the FB/SC-IVR method requires the evaluation of quite a large number of trajectories ($\sim 10^6$ trajectories), and of course will be even more demanding for systems with many more degrees of freedom, but together with stationary phase MC and other smoothing methods under development, is expected to provide a more tractable approach. However, this remains to be demonstrated by substantial applications of the present methodology to studies of reaction dynamics in polyatomic systems.

ACKNOWLEDGMENTS

W.H.M. gratefully acknowledges financial support from the Director, Office of Energy Research, Office of Basic Energy Sciences, Chemical Sciences Division of the U.S. Department of Energy under Contract No. DE-AC03-76SF00098, by the Laboratory Directed Research and Development (LDRD) project from the National Energy Research Scientific Computing Center (NERSC), Lawrence Berkeley National Laboratory, and by the National Science Foundation under Grant No. CHE-9732758. W.H.M. also acknowledges a generous allocation of supercomputing time from the National Energy Research Scientific Computing Center (NERSC). D.M.N. acknowledges support by the National Science Foundation under Grant No. CHE-9710243.

[1] L. R. Khundkar and A. H. Zewail, Annu. Rev. Phys. Chem. **41**, 15 (1990).
[2] A. H. Zewail, J. Phys. Chem. **97**, 12427 (1993).
[3] J. C. Polanyi and A. H. Zewail, Acc. Chem. Res. **28**, 119 (1995).
[4] *Femtosecond Chemistry*, edited by J. Manz and L. Woste (VCH, Weinheim, 1995).
[5] *Ultrafast Phenomena IX*, edited by P. F. Barbara *et al.* (Springer, Berlin, 1994).
[6] T. Baumert, B. Buhler, M. Grosser, R. Thalweiser, V. Weiss, E. Wiedenmann, and G. Gerber, J. Phys. Chem. **95**, 8103 (1991).
[7] M. Dantus, M. H. M. Janssen, and A. H. Zewail, Chem. Phys. Lett. **181**, 281 (1991).
[8] M. T. Zanni, T. R. Taylor, B. J. Greenblatt, B. Soep, and D. M. Neumark, J. Chem. Phys. **107**, 7613 (1997).
[9] P. Ludowise, M. Blackwell, and Y. Chen, Chem. Phys. Lett. **258**, 530 (1996).
[10] A. Assion, M. Geisler, J. Helbing, V. Seyfried, and T. Baumert, Phys. Rev. A **54**, R4605 (1996).
[11] C. Meier and V. Engel, J. Chem. Phys. **101**, 2673 (1994).
[12] C. Meier and V. Engel, Chem. Phys. Lett. **212**, 691 (1993).
[13] W. Radloff, V. Stert, Th. Freudenberg, and I. V. Hertel, Chem. Phys. Lett. **281**, 20 (1997).
[14] T. Baumert, J. L. Herek, and A. H. Zewail, J. Chem. Phys. **99**, 4430 (1993).
[15] P. Y. Cheng, D. Zhong, and A. H. Zewail, Chem. Phys. Lett. **237**, 399 (1995).
[16] B. J. Greenblatt, M. T. Zanni, and D. M. Neumark, Science **276**, 1675 (1997).
[17] B. J. Greenblatt, M. T. Zanni, and D. M. Neumark, Chem. Phys. Lett. **258**, 523 (1996).
[18] I. Fischer, M. J. J. Vrakking, D. M. Villeneuve, and A. Stolow, Chem. Phys. **207**, 331 (1996).
[19] I. Fischer, D. M. Villeneuve, M. J. J. Vrakking, and A. Stolow, J. Chem. Phys. **102**, 5566 (1995).
[20] W. H. Miller, J. Chem. Phys. **53**, 3578 (1970).
[21] E. J. Heller, J. Chem. Phys. **94**, 2723 (1991).
[22] E. J. Heller, J. Chem. Phys. **95**, 9431 (1991).
[23] K. G. Kay, J. Chem. Phys. **100**, 4377 (1994).
[24] K. G. Kay, J. Chem. Phys. **100**, 4432 (1994).
[25] K. G. Kay, J. Chem. Phys. **101**, 2250 (1994).
[26] M. F. Herman and E. Kluk, Chem. Phys. **91**, 27 (1984).
[27] E. Kluk, M. F. Herman, and H. L. Davis, J. Chem. Phys. **84**, 326–334 (1986).
[28] A. R. Walton and D. E. Manolopoulos, Mol. Phys. **87**, 961 (1996).
[29] M. L. Brewer, J. S. Hulme, and D. E. Manolopoulos, J. Chem. Phys. **106**, 4832 (1997).
[30] G. Campolieti and P. Brumer, Phys. Rev. A **50**, 997 (1994).
[31] G. Campolieti and P. Brumer, J. Chem. Phys. **96**, 5969 (1992).
[32] G. Campolieti and P. Brumer, J. Chem. Phys. **107**, 791 (1997).
[33] S. Keshavamurthy and W. H. Miller, Chem. Phys. Lett. **218**, 189 (1994).
[34] S. Garashchuk and D. J. Tannor, Chem. Phys. Lett. **262**, 477 (1996).
[35] F. Grossmann, Chem. Phys. Lett. **262**, 470 (1996).
[36] K. G. Kay, J. Chem. Phys. **107**, 2313 (1997).
[37] V. S. Batista and W. H. Miller, J. Chem. Phys. **108**, 498 (1998).
[38] N. T. Maitra and E. J. Heller, Phys. Rev. Lett. **78**, 3035 (1997).
[39] B. Spath and W. H. Miller, J. Chem. Phys. **104**, 95 (1996).
[40] A. R. Walton and D. E. Manolopoulos, Chem. Phys. Lett. **244**, 448 (1995).
[41] X. Sun and W. H. Miller, J. Chem. Phys. **106**, 6346 (1997).
[42] H. B. Wang, X. Sun, and W. H. Miller, J. Chem. Phys. **108**, 9726 (1998).
[43] X. Sun and W. H. Miller, J. Chem. Phys. **108**, 8870 (1998).
[44] D. V. Shalashilin and B. Jackson, Chem. Phys. Lett. **291**, 143 (1998).
[45] R. Bersohn and A. H. Zewail, Ber. Bunsenges. Phys. Chem. **92**, 373 (1988).
[46] S. Y. Lee, W. T. Pollard, and R. A. Mathies, J. Chem. Phys. **90**, 6146 (1989).
[47] R. E. Walkup, J. A. Misewich, J. H. Glownia, and P. P. Sorokin, J. Chem. Phys. **94**, 3389 (1991).

[48] M. Ovchinnikov and V. A. Apkarian, J. Chem. Phys. **105**, 10312 (1996).
[49] M. Ovchinnikov and V. A. Apkarian, J. Chem. Phys. **106**, 5775 (1997).
[50] M. Ovchinnikov and V. A. Apkarian, J. Chem. Phys. **108**, 2277 (1998).
[51] V. Engel, H. Metiu, R. A. Marcus, and A. H. Zewail, Chem. Phys. Lett. **152**, 1 (1988).
[52] S. O. Williams and D. G. Imre, J. Phys. Chem. **92**, 6636 (1988).
[53] V. Engel and H. Metiu, J. Chem. Phys. **90**, 6116 (1989).
[54] V. Engel and H. Metiu, J. Chem. Phys. **91**, 1596 (1989).
[55] S. H. Lin and B. Fain, Chem. Phys. Lett. **155**, 216 (1989).
[56] B. Fain, S. H. Lin, and W. X. Wu, Phys. Rev. A **40**, 824 (1989).
[57] S. Y. Lee, W. T. Pollard, and R. A. Mathies, Chem. Phys. Lett. **160**, 531 (1989).
[58] S. Mukamel, *Principles of Nonlinear Optical Spectroscopy* (Roxford University Press, New York, 1995).
[59] A. M. Walsh and R. F. Loring, Chem. Phys. Lett. **160**, 299 (1989).
[60] B. Fain and S. H. Lin, J. Chem. Phys. **93**, 6387 (1990).
[61] W. Vogel, D. G. Welsch, and B. Wilhelmi, Phys. Rev. A **37**, 3825 (1987).
[62] M. Mitsunaga and C. L. Tang, Phys. Rev. A **35**, 1720 (1987).
[63] J. A. Yeazell, M. Mallalieu, J. Parker, and C. R. Stroud Jr., Phys. Rev. A **40**, 5040 (1989).
[64] V. Engel, Chem. Phys. Lett. **178**, 130 (1991).
[65] V. Engel and H. Metiu, Chem. Phys. Lett. **155**, 77 (1989).
[66] M. Seel and W. Domcke, Chem. Phys. **151**, 59 (1991).
[67] J. Faeder, N. Delaney, P. E. Maslen, and R. Parson, Chem. Phys. Lett. **270**, 196 (1997).
[68] M. Seel and W. Domcke, J. Chem. Phys. **95**, 7806 (1991).
[69] M. Braunstein, P. J. Hay, R. L. Martin, and R. T. Pack, J. Chem. Phys. **95**, 8239 (1991).
[70] M. Braun, C. Meier, and V. Engel, J. Chem. Phys. **103**, 7907 (1995).
[71] R. Kosloff, J. Phys. Chem. **92**, 2086 (1988).
[72] G. Stock and M. Thoss, Phys. Rev. Lett. **78**, 578 (1997).
[73] S. A. Pentidis and R. F. Loring, Chem. Phys. Lett. **287**, 217 (1998).
[74] N. Makri and K. Thompson, Chem. Phys. Lett. **291**, 101 (1998).
[75] R. Kosloff, J. Phys. Chem. **92**, 2087 (1988).
[76] E. C. M. Chen and W. E. Wentworth, J. Phys. Chem. **89**, 4099 (1985).
[77] J. G. Dojahn, E. C. M. Chen, and W. E. Wentworth, J. Phys. Chem. **100**, 9649 (1996).
[78] E. C. M. Chen, J. G. Dojahn, and W. E. Wentworth, J. Phys. Chem. **101**, 3088 (1997).
[79] P. W. Tasker, G. G. Balint-Kurti, and R. N. Dixon, Mol. Phys. **32**, 1651 (1976).
[80] G. A. Bowmaker, P. Schwerdfeger, and L. V. Szentpaly, J. Mol. Struct.: THEOCHEM **53**, 87 (1989).
[81] D. Danonvich, J. Hrusak, and S. Shaik, Chem. Phys. Lett. **233**, 249 (1995).
[82] P. E. Maslen, J. Faeder, and R. Parson, Chem. Phys. Lett. **263**, 63 (1996).
[83] P. Luc, J. Mol. Spectrosc. **80**, 41 (1980).
[84] S. Churrasy, F. Martin, R. Bacis, J. Verges, and R. W. Field, J. Chem. Phys. **75**, 4863 (1981).
[85] J. Tellinghuisen, J. Chem. Phys. **82**, 4012 (1985).
[86] K. S. Viswanathan, A. Sur, and J. Tellinghuisen, J. Mol. Spectrosc. **86**, 393 (1981).
[87] J. Tellinghuisen, J. Mol. Spectrosc. **94**, 231 (1982).
[88] K. S. Viswanathan and J. Tellinghuisen, J. Mol. Spectrosc. **101**, 285 (1983).
[89] A. L. Guy, A. Sur K. S. Viswanathan, and J. Tellinghuisen, Chem. Phys. Lett. **73**, 582 (1980).
[90] Le Roy, J. Chem. Phys. **52**, 2683 (1970).
[91] W. A. de Jong, L. Visscher, and W. C. Nieuwpoort, J. Chem. Phys. **107**, 9046 (1997).
[92] M. Saute and M. Aubert-Frecon, J. Chem. Phys. **77**, 5639 (1982).
[93] E. P. Gordeev, S. Ya. Umansky, and A. I Voronin, Chem. Phys. Lett. **23**, 524 (1973).
[94] R. Mulliken, J. Chem. Phys. **55**, 288 (1971).
[95] W. H. Press, B. P. Flannery, S. A. Teukolsky, and W. T. Vetterling, in *Numerical Recipes* (Cambridge University Press, Cambridge, 1986).
[96] V. S. Batista and D. F. Coker, J. Chem. Phys. **105**, 4033 (1996).
[97] V. S. Batista and D. F. Coker, J. Chem. Phys. **106**, 6923 (1997).
[98] V. S. Batista and D. F. Coker, J. Chem. Phys. **106**, 7102 (1997).